# Contents

Table 1 contains an overview of all symbols used in this lab report.

| Symbol | Meaning |
| --- | --- |
| $A$ | Area |
| $B$ | Magnetic field strength |
| $c$ | Speed of light |
| $D$ | Lengths |
| $E$ | Energy |
| $\boldsymbol{E}$ | Electric field |
| $e$ | Electric charge |
| $F$ | Field-flux-coefficient |
| $H$ | Magnetic field strength |
| $\hbar$ | Planck constant |
| $I$ | Current |
| $\boldsymbol{j}$ | Current density |
| $L$ | Lengths |
| $m$ | mass |
| $n_e$ | Charge density |
| $p$ | Magnetic dipole moment |
| $R$ | Resistance |
| $r$ | Radius |
| $S$ | Spin |
| $T$ | Temperature |
| $t$ | Time |
| $U$ | Voltage |
| $\boldsymbol{v}$ | Velocity |
| $z$ | Distance between used object and SQUID sensor |
| $\mu_0$ | Magnetic field constant |
| $\Phi$ | Magnetic flux |
| $\phi$ | angle |
| $\omega$ | Angular velocity |
| $\alpha, \beta, \gamma, \delta$ | Fit parameters |
| $s_x$ | Uncertainty of the value $x$ |

Table 1: Symbols used in this lab report.

# 1   Introduction

In this experiment the dipole moment of different samples shall be determined using a SQUID (Superconducting Quantum Interference Device). An RF-Squid is used, which consists of a superconducting ring with a Josephson junction. With this setup it is possible to detect very low magnetic field strengths.

## 2  Physical basics

The theoretical principles described below are based on the Staatsexamen [1] and the instructions [2].

### 2.1  Superconductivity

Superconductors can be characterized by some properties, which are briefly explained in the following. Below the material-dependent critical temperature $T_c$, the electrical resistance of a superconductor drops to a value that is immeasurably small. Furthermore, superconductors in the superconducting state behave like ideal diamagnet. This means that almost no magnetic field can penetrate the superconductor. This behaviour is explained by the Meissner-Ochsenfeld effect. In addition, superconductors reveal a temperature-dependent energy gap

$$E_g = E_f \pm \Delta E, \tag{1}$$

where $E_F$ refers to the Fermi energy. This property can be described by the BCS-Theory, which will be discussed later. Below the critical temperature, electrons of the superconductor change into a macroscopic quantum state in which cooper pairs are formed. Superconductivity in superconductors can be interrupted even at a temperature below the critical temperature: This can be caused by strong external magnetic fields, large currents or an alternating electromagnetic field withe a frequency of the order of $\frac{\Delta E}{\hbar}$.

Superconductors can be divided into two different types. The first type of superconductors have a maximum critical temperature of $T_c = 23.2\,\text{K}$. These superconductors have a material-dependent critical magnetic field strength $H_c$ at which the superconductivity is broken. At magnetic field strengths below $H_c$ the magnetic field can penetrate just a few nanometers into the superconductor. In the second type of superconductors, also know as high-temperature superconductors, superconductivity can be achieved at temperatures of up to $200\,\text{K}$. These superconductors have two critical magnetic field strengths. At $H_{c2}$ the magnetic field is only partially displaced and at $H_{c1}$ it vanishes completely.

### 2.2  London equations

As mentioned before, a magnetic field can only penetrate a few nanometers into a superconductor. This penetration depth can be determined using the London equations. For the calculation it must be assumed that $m\dot{\boldsymbol{v}}_e = -e\boldsymbol{E}$ applies. If this condition is met and the definition of the current density $\boldsymbol{j} = n_e e \boldsymbol{v}_e$, of a charge density $n_e$, is applied to the Maxwell equations, the following term can be obtained:

$$\frac{\partial}{\partial t}\left(\nabla \times \boldsymbol{j} + \frac{n_e e^2}{mc}\boldsymbol{B}\right) = 0. \tag{2}$$

Since within a superconductor $B = 0$ must apply, the term in the brackets in the equation shown above must be zero for any time leading to the London equation

$$\nabla \times \boldsymbol{j} = -\frac{n_e e^2}{mc} \boldsymbol{B}. \tag{3}$$

From which the two London equations

$$\nabla^2 \boldsymbol{B} = \frac{4\pi n_e e^2}{mc^2} \boldsymbol{B} \tag{4}$$

$$\nabla^2 \boldsymbol{j} = \frac{4\pi n_e e^2}{mc^2} \boldsymbol{j} \tag{5}$$

can be derived. These equations are solved by exponentially decaying functions which provide the penetration depth $\Lambda = \sqrt{\frac{mc^2}{4\pi n_e e^2}}$.

## 2.3   BCS theory

The conductive behaviour of superconductors with a temperature below $T_\mathrm{c}$ can mainly be described by the BCS theory. Unlike metallic conductors, the current is not carried by individual free electrons, but by bound electron pairs, so-called cooper pairs. The protons in the atomic lattice have a high inertia compared to the electrons. Thus, an electron leaves a positive polarization trace attracting another electron. The coupling of the electron pair is formed by this effect. Since electrons are fermions, meaning that two electrons must not be in the same state, the electrons of a cooper pair have opposite spins. This leads to the condition that a cooper pair can be understood as a quasi-particle with an integer spin of $S = 0$. Due to the integer spin, a cooper pair has boson characteristics, so it is subject to Bose-statistics. Thus, the cooper pairs can assume an energetically lower state and due to the boson properties, several cooper pairs are allowed to be in the same state. This leads to a lower total energy of the system, which results in a drop in the resistance of a superconductor, making it superconducting.

## 2.4   Flux quantization

In this experiment, a ring-shaped superconductor is used. Therefore the circuit current can be calculated as a closed path over the current density $\boldsymbol{j}$ and since the current is constant,

$$0 = \oint \boldsymbol{j} d\boldsymbol{l} \tag{6}$$

applies. According to Stoke's theorem, the magnetic flux $\Phi_B$ through the ring can be calculated with

$$\oint \boldsymbol{A} \cdot \mathrm{d}\boldsymbol{l} = \Phi_B. \tag{7}$$

Since the phase of the wave function of the cooper pairs is a well defined parameter, the result can only change by a multiple of $2\pi$ after one revolution. From that follows:

$$\oint \nabla\theta d\boldsymbol{l} = \Delta\theta = 2\pi n \tag{8}$$

This results in a quantization of the magnetic flux in fluxon $\Phi_0$ of the form:

$$|\Phi_B| = n\frac{\hbar}{2e} = n\Phi_0, \tag{9}$$

with

$$\Phi_0 = 2.067\,833\,667 \times 10^{-15}\,\text{Wb}. \tag{10}$$

## 2.5   Josephson effect

If a superconductor is interrupted by a thin insulating layer, the cooper pairs can still tunnel through this layer. This phenomenon is called Josephson effect and such an insulator layer is called Josephson junction. The wave functions of the cooper pairs to the left and right of the isolator must merge continuously. As a result, the tunnel current depends only on the phase shift. This means that the cooper pairs do not lose any energy during tunneling, so that no current drops in the insulator, even if it is not a superconductor. Since the insulator is not a superconductor, a magnetic field can penetrate the insulator layer. This causes a phase shift, which results in the Josephson direct current:

$$I = I_0 \frac{\sin \pi\Phi/\Phi_0}{\pi\Phi/\Phi_0}. \tag{11}$$

## 2.6   The magnetic field of a conductor loop

The magnetic field in $z$-direction $B_z$ of a conductor loop can be calculated with

$$B_z = \frac{\mu_0 p}{2\pi z^3}, \tag{12}$$

where $\mu_0$ is the magnetic field constant, $z$ the distance in the $z$-direction of the conductor loop and $p$ the magnetic dipole moment. The magnetic dipole moment can be calculated with

$$p = A\frac{U}{R}, \tag{13}$$

where $U$ is the voltage and $R$ the resistance applied to the loop and $A$ the area enclosed by the conductor loop. $A$ can be calculated with $\pi r^2$, where $r$ is the radius of the conductor loop. The magnetic field can also be calculated from the

measurements of the SQUID. The measured voltage $U$ of the circuit can be converted into the magnetic field strength using

$$B_z = F\frac{\Delta U}{s_i}.$$                                               (14)

$F$ is the field-flux-coefficient which is specified as $F = 9.3\,\mathrm{nT}/\Phi_0$ [2, p. 21] for the used SQUID and $s_i[\mathrm{V}/\Phi_0]$ is the used value of the feedback-resistor. The magnetic dipole moment can be calculated with

$$p = \frac{2\pi}{\mu_0}B_z z^3$$                                              (15)

from the magnetic field strength obtained.

# 3 Setup and procedure

## 3.1 Setup
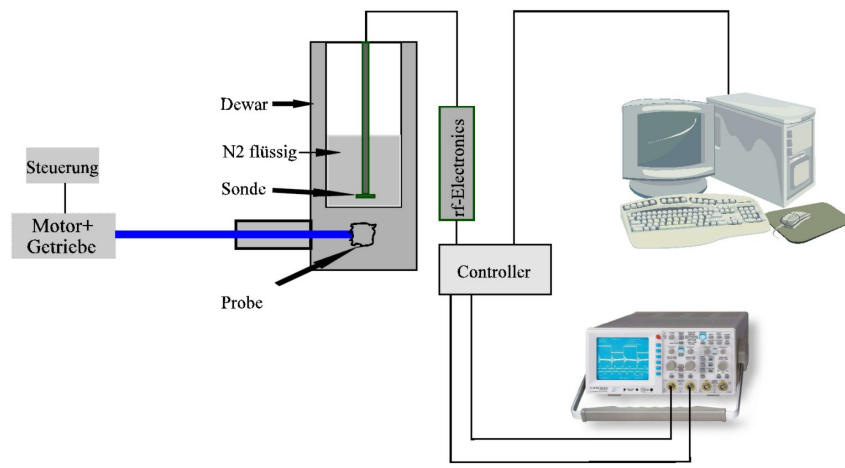


Figure 1: Schematic representation of the structure used in the experiment. [2, p.19]

A schematic representation of the experimental setup is shown in fig. 1. The main part of the experiment is the RF-SQUID: The core element is a SQUID sensor which consists of a superconductor ring interrupted by a Josephson contact. In order for the temperature of the sensor to be below the critical temperature, it is located in a cylinder filled with liquid nitrogen. Above the SQUID sensor, there is an LC circuit which generates an additional magnetic flux. The voltage of the circuit is the actual measured parameter in this experiment. The controller of the circuit can be set via a computer and the signal of the circuit can be viewed via an oscilloscope, which in turn can then be read out by the computer. The samples producing the magnetic field can be placed below the sensor using a carriage and rotated using a motor. Different angular velocities can be set on the motor. The samples are once a conductor loop in which different resistances can be set and a collection of different objects.

## 3.2 Procedure

**Calibration**

First, the length of the bar to which the SQUID sensor is attached was measured using a ruler. The sensor was then placed in the cylinder after which we waited 15 minutes for the sensor to cool down sufficiently. Then, all devices were switched on and the program JSQ Duo Sensor Control was started on the computer with which the circuit could be controlled. The program was set to the test mode, in which a triangle voltage is coupled into the circuit. At the oscilloscope, the triangle

voltage as well as the SQUID signal could be observed. In order to calibrate the oscilloscope correctly, the VCA (amplitude of current) was set to 1000 and the VCO (frequency of current) parameter was varied until the value was found for which the voltage of the SQUID signal was at its maximum. Afterwards, the VCA was set so that the SQUID signal became maximum again. In addition, by varying the offset, the SQUID signal was shifted to the center of the oscilloscope screen. After the calibration was completed, the program was switched to the measuring mode. On the first day, no proper signal long enough to carry out the measurements could be found. On the second day we first waited until the sensor was cooled down again and then started the calibration. At first, no signal could be found again. After taking the SQUID sensor out of the cylinder, blow-drying it and then cooling it down in the cylinder, a new calibration could be carried out. After the calibration however, we were able to measure a signal with the set parameters VCA = 1061, VCO = 1390 and OFF = 1840. The resulting SQUID pattern is shown in fig. 2.
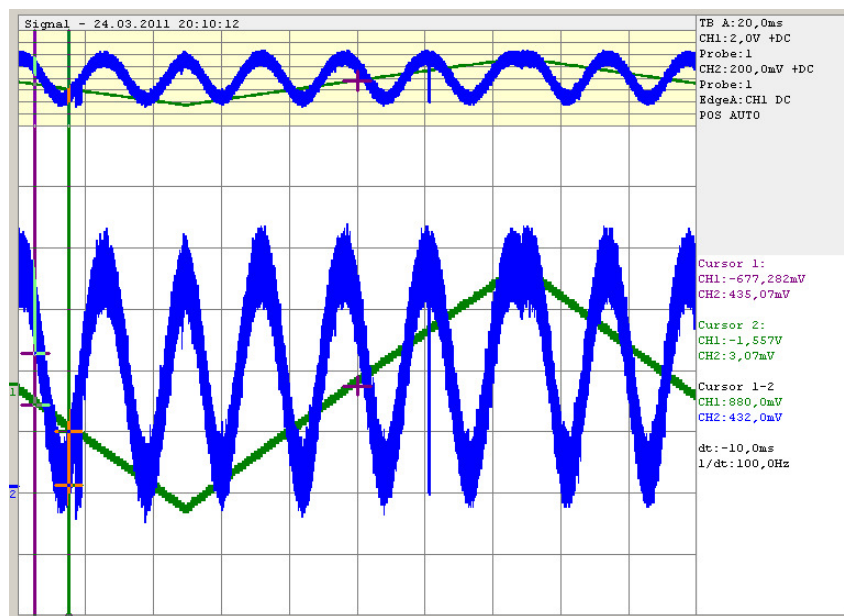


Figure 2: The SQUID pattern obtained during calibration.

**Measurement**

The first step was to measure with the conductor loop. For each of the five resistors, the SQUID signal was measured with three different angular velocities $\omega = 2, 5, 10$ where $\omega$ refers to the name of the motor setting. During measurements, we noted that the higher the resistance, the worse the SQUID signal became. The data of each measurement was saved on the computer as .csv and .bmp files. During the measurements with the conductor loop, the integration capacitance was set to

$100\,\mathrm{nF}$ and the resistance of the circuit was set to $100\,\mathrm{K}$. Afterwards, seven more samples were measured: The samples were a grey stone, a reddish stone, an iron span, a magnetic span, a gold sample, a crown cap and an iron rod. For all these measurements, the angular velocity was set to $\omega = 5$. The integration capacity had to be changed several times for the different samples and the resistance of the circuit had to be reduced for the crown cap and the iron rod. The exact settings can be seen in the laboratory note in the appendix (cf. appendix A). Finally, the radius $r$ of the conductor loop, the distance from the conductor loop to the top of the cylinder and the voltage applied to the conductor loop were measured. After this, the experiment was finished and the SQUID sensor was taken out of the cylinder again and blow-dried, as wetness can damage the SQUID.

## 4 Analysis

### 4.1 Theoretical calculation of the magnetic field and magnetic dipole moment

Firstly, the theoretical value for the magnetic field of the conductor loop is calculated. For that, the distance between the conductor loop and the SQUID sensor has to be calculated. The distance of the conductor loop to the top of the cylinder was measured to be $L = (29.0 \pm 0.1)\,\text{cm}$, a red marking on the cylinder was used for the position of the conductor loop. For the distance of the SQUID sensor to the top of the cylinder, the values $\bar{D} = (24.9 \pm 0.4) \times 10^{-2}\,\text{m}$ were obtained using seperate measurements taken with a ruler: This distance was measured twice and the mean of both measurements was calculated. The measured values and estimated uncertainties can be found in the laboratory notes in the appendix appendix A. The uncertainty of the mean was calculated with Gaussian error propagation:

$$s_{\bar{D}} = \frac{1}{2}\sqrt{s_{D1}^2 + s_{D2}^2}. \tag{16}$$

This results in a distance between conductor loop and SQUID of $z = (4.1 \pm 0.4)\,\text{cm}$ where the uncertainty again was calculated with Gaussian error propagation.

As the conductor loop wasn't formed uniformly, the diameter of the conductor loop was measured three times and half of the values were taken to obtain the radius $r$. Again, the mean was calculated which results in a value of $r = (2.12 \pm 0.06)\,\text{mm}$ for the radius. At last, the voltage applied to the conductor loop is required, which has also been measured several times. For the uncertainty of the voltage measurements, the uncertainty of $0.5\,\%$ of the measured value plus one digit specified by the manufacturer was assumed. The mean was calculated with the result of $\bar{U} = (2.408 \pm 0.010)\,\text{V}$. Now the magnetic field of the conductor loop for the different resistors could be calculated with eq. (12). The values obtained are shown in table 2. The uncertainties of the magnetic field strengths were calculated with

$$s_B = \frac{\mu_0}{2}\sqrt{\left(\frac{r^2}{Rz^3}s_U\right)^2 + \left(\frac{2Ur}{Rz^3}s_r\right)^2 + \left(\frac{Ur^2}{R^2z^2}s_R\right)^2 + \left(\frac{3Ur^2}{Rz^4}s_z\right)^2}. \tag{17}$$

Additionally, the magnetic dipole moments were calculated with eq. (13). Since $A = \pi r^2$, the uncertainty of $A$ can be calculated as $s_A = 2\pi r s_r$. With this the uncertainty of the dipole moment is calculated to

$$s_p = \sqrt{\left(\frac{U}{R}s_A\right)^2 + \left(\frac{A}{R}s_U\right)^2 + \left(\frac{AU}{R^2}s_R\right)^2}. \tag{18}$$

The calculated dipole moments are also shown in table 2.

For comparison and later error analysis, the distance between the conductor loop and the top of the cylinder was determined in an alternative way by measuring the distance from the sample inlet to the cylinder cover. This leads to the distance $z_2 = (4.4 \pm 0.4)\,\text{cm}$. The magnetic field strength was also calculated with this distance in the same way as explained above; the results are shown in table 2.

| Resistor | $R/\Omega$ | $B/\text{nT}$ | $B_2/\text{nT}$ | $p/\text{nA}\,\text{m}^2$ |
|----------|------------|---------------|-----------------|---------------------------|
| R1 | $51.47 \pm 0.05$ | $4.9 \ \pm 1.8$ | $1.49 \ \pm 0.03$ | $660 \ \pm 40$ |
| R2 | $100.80 \pm 0.10$ | $2.5 \ \pm 0.9$ | $0.76 \ \pm 0.02$ | $336 \ \pm 18$ |
| R3 | $300.8 \ \pm 0.3$ | $0.8 \ \pm 0.3$ | $0.256 \pm 0.007$ | $113 \ \pm 6$ |
| R4 | $510.6 \ \pm 0.5$ | $0.49 \pm 0.18$ | $1.507 \pm 0.004$ | $66 \ \pm 4$ |
| R5 | $1000.0 \ \pm 1.0$ | $0.25 \pm 0.09$ | $0.769 \pm 0.002$ | $33.9 \pm 1.9$ |

Table 2: The theoretical values for the magnetic field $B$ and the magnetic dipole moment $p$ of the conductor loop with various set resistors calculated from the measured distance between conductor loop and SQUID sensor and the measured radius of the conductor loop.

## 4.2   Calculation of the magnetic field with the SQUID data

For each measurement with the conductor loop, a sine fit of the form

$$U_i = \alpha \sin\left(\beta \cdot t_i + \gamma\right) + \delta \tag{19}$$

was applied to the data. In the above equation, $\alpha, \beta, \gamma$ and $\delta$ are parameters to be determined by the fit while $U_i$ and $t_i$ refer to the data given by the oscilloscope. The Python module `scipy.optimize.curve_fit` was used for the fits. Figure 3 shows an exemplary plot of the measured data and the sine fit for the set resistance R1 and the angular velocity $\omega = 2$. For the remaining measurements, the plots can be found in the appendix. In order to be able to check the quality of the fits, the coefficient of determination $R^2$ was calculated for each fit with:

$$R^2 = 1 - \frac{\sum_i(U_i - [\alpha \sin\left(\beta \cdot t_i + \gamma\right) + \delta])^2}{\sum_i(U_i - \bar{U})^2}, \tag{20}$$

where $U_i$ is the measured voltage and $\bar{U}$ is the mean of the measured voltages. The magnetic field strength can be calculated from the fit parameter $\alpha$ using eq. (14). For the magnetic field strengths of the conductor loop $s_i = 1.9\,\text{V}/\Phi_0$. The obtained magnetic field strengths are shown in table 3. The uncertainties of the calculated strengths results from

$$s_B = F\frac{s_\alpha}{s_i}. \tag{21}$$

With these field strengths, the magnetic dipole moment can be calculated additionally with eq. (15). The uncertainty for these results can be calculated with

$$s_p = \frac{2\pi}{\mu_0}\sqrt{\left(3B_z z^2 s_z\right)^2 + \left(z^3 s_B\right)^2}. \tag{22}$$

The obtained results are also shown in table 3. The magnetic dipole moments were calculated with both distances $z$ and $z_2$. For each resistor the mean of the field strength and the dipole moment for the different angular velocities was calculated,
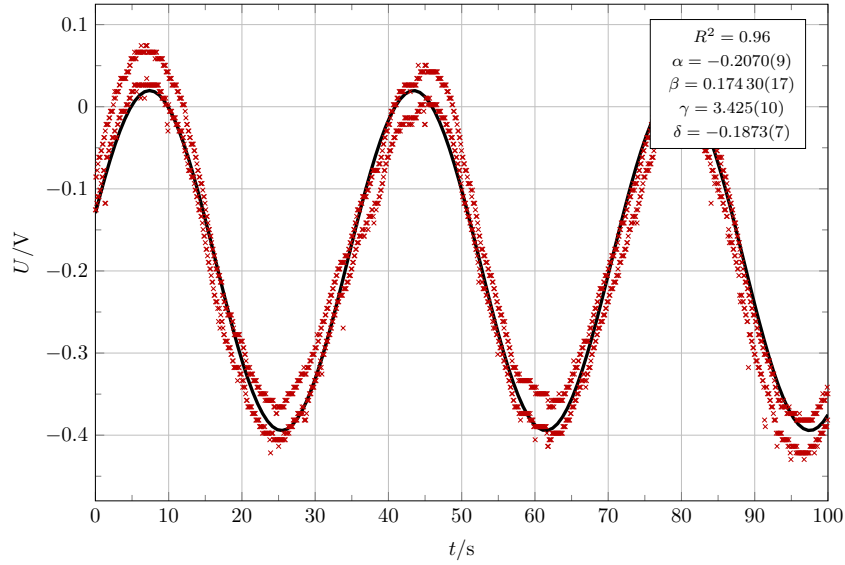
Figure 3: The measured data and the applied sinus fit for the measurement with R1 and $\omega = 2$.

which can be seen in table 4. For the measurements of the other objects, a sine fit was carried out with the same method as for the conductor loop. From this, the magnetic field strengths and the magnetic dipole moments were calculated in the same way as described above. For the iron stick and the crown cap the resistance of the circuit had to be reduced. Therefore, for the calculation for the iron stick $s_i = 0.38 \, \text{V}/\Phi_0$ and for the crown cap $s_i = 0.06 \, \text{V}/\Phi_0$ was used. The plots showing the data and the fits can be found in the appendix while the calculated magnetic field strengths and magnetic dipole moments are shown in table 5.

## 4.3 Polar plots of the measured magnetic fields

To be able to draw the polar plots, the time measured by the oscilloscope had to be converted to an angle $\alpha$ using

$$\phi = \beta \cdot t + \gamma \tag{23}$$

where $\beta$ and $\gamma$ refer to the parameters of the respective fit (cf. eq. (19)). Also, the measured magnetic field had to be converted to the absolute value of the magnetic field strength with the equation

$$|B| = |U - \delta| \cdot \frac{F}{s_i}. \tag{24}$$

With that, the polar plots could be drawn. The polar plot for the measurement with resistance R2 and the angular velocity $\omega = 2$ is shown in fig. 4. The remaining plots can be found in the appendix.

| Resistor | Rotation | $B/\mathrm{nT}$ | $p/\mathrm{nA\,m^2}$ | $p_2/\mathrm{nA\,m^2}$ |
|---|---|---|---|---|
| R1 | 2 | $1.013 \pm 0.005$ | $140 \pm 50$ | $430 \pm 120$ |
| R1 | 5 | $1.006 \pm 0.005$ | $140 \pm 50$ | $430 \pm 120$ |
| R1 | 10 | $0.992 \pm 0.004$ | $130 \pm 50$ | $420 \pm 120$ |
| R2 | 2 | $0.478 \pm 0.004$ | $60 \pm 30$ | $200 \pm 60$ |
| R2 | 5 | $0.526 \pm 0.005$ | $70 \pm 30$ | $220 \pm 60$ |
| R2 | 10 | $0.547 \pm 0.004$ | $70 \pm 30$ | $230 \pm 60$ |
| R3 | 2 | $0.237 \pm 0.004$ | $32 \pm 13$ | $100 \pm 30$ |
| R3 | 5 | $0.168 \pm 0.004$ | $23 \pm 9$ | $70 \pm 20$ |
| R3 | 10 | $0.248 \pm 0.003$ | $34 \pm 13$ | $100 \pm 30$ |
| R4 | 2 | $0.102 \pm 0.003$ | $14 \pm 6$ | $43 \pm 12$ |
| R4 | 5 | $0.153 \pm 0.002$ | $21 \pm 8$ | $65 \pm 18$ |
| R4 | 10 | $0.103 \pm 0.004$ | $14 \pm 6$ | $44 \pm 12$ |
| R5 | 2 | $0.107 \pm 0.002$ | $15 \pm 6$ | $48 \pm 13$ |
| R5 | 5 | $0.087 \pm 0.004$ | $12 \pm 5$ | $37 \pm 10$ |
| R5 | 10 | $0.093 \pm 0.003$ | $13 \pm 5$ | $40 \pm 11$ |

Table 3: The measured values for the magnetic field $B$ and the magnetic dipole moment $p$ of the conductor loop with various set resistors and angular velocity.

| Resistor | $B/\mathrm{nT}$ | $p/\mathrm{nA\,m^2}$ | $p_2/\mathrm{nA\,m^2}$ |
|---|---|---|---|
| R1 | $1.004 \pm 0.003$ | $140 \pm 30$ | $430 \pm 70$ |
| R2 | $0.517 \pm 0.003$ | $70 \pm 16$ | $220 \pm 30$ |
| R3 | $0.218 \pm 0.002$ | $29 \pm 7$ | $90 \pm 15$ |
| R4 | $0.1193 \pm 0.0019$ | $16 \pm 3$ | $50 \pm 8$ |
| R5 | $0.0958 \pm 0.0018$ | $13 \pm 3$ | $40 \pm 6$ |

Table 4: The average values for $B$ and $p$ for the respective resistor.

| Samples | $B/\mathrm{T}$ | $p/\mathrm{A\,m^2}$ | $p_2/\mathrm{A\,m^2}$ |
|---|---|---|---|
| Iron span | $3.3 \pm 0.3 \times 10^{-11}$ | $4.4 \pm 1.8 \times 10^{-9}$ | $1.4 \pm 0.4 \times 10^{-9}$ |
| Gold | $5.4 \pm 0.6 \times 10^{-11}$ | $7 \pm 3 \times 10^{-9}$ | $2.3 \pm 0.7 \times 10^{-9}$ |
| Gray stone | $1.67 \pm 0.06 \times 10^{-10}$ | $2.3 \pm 0.9 \times 10^{-8}$ | $7.1 \pm 2.0 \times 10^{-8}$ |
| Iron stick | $6.37 \pm 0.07 \times 10^{-8}$ | $9 \pm 3 \times 10^{-6}$ | $2.7 \pm 0.7 \times 10^{-5}$ |
| Crown cap | $9.36 \pm 0.05 \times 10^{-7}$ | $1.3 \pm 0.5 \times 10^{-4}$ | $4.0 \pm 1.1 \times 10^{-4}$ |
| Magnetic span | $1.989 \pm 0.006 \times 10^{-8}$ | $2.7 \pm 1.1 \times 10^{-6}$ | $8 \pm 2 \times 10^{-6}$ |
| Red stone | $5.94 \pm 0.08 \times 10^{-10}$ | $8 \pm 3 \times 10^{-8}$ | $2.5 \pm 0.7$ |

Table 5: The measured values for $B$ and $p$ for the different samples.
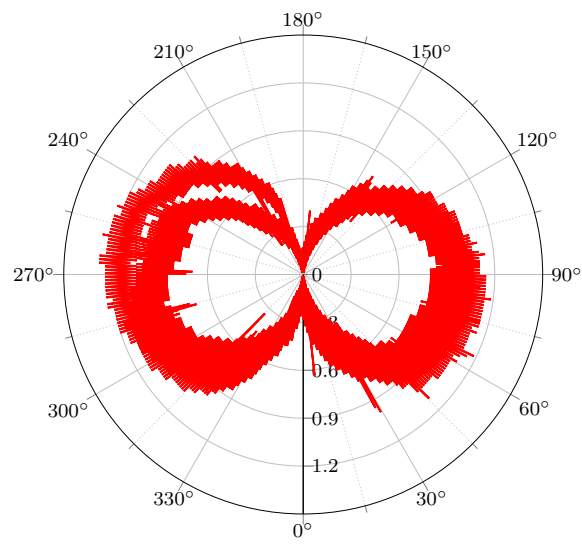
Figure 4: Polar plot of the measurement with R1 and $\omega = 2$

## 5 Discussion

The measurement with the conductor loop shows that the magnetic field strength and magnetic dipole moment decrease for larger resistances, as expected. We also noted that the quality of the signal decreases greatly with higher resistances: As the plots show, the signal for higher resistances does not clearly correspond to the expected sine shape, which is also shown by the smaller $R^2$ values for higher resistances. Also, the polar plots do not show the expected eight-like shape at high resistances. The same effect can also be seen from the measurements of the other objects: The stronger their magnetic fields become, the clearer the sine shape of the signals and the clearer the eight like shape of the polar plot get. The measurements with the magnetic span, the crown cork and the iron rod which have by far the strongest magnetic fields have a very clear sine signal.

For comparison, the theoretical magnetic field strengths and those measured are show in table 6. The values for the magnetic dipole moment are shown in table 7.

| Resistor | $B_{\text{theo}}/\text{nT}$ | $B_{2,\text{theo}}/\text{nT}$ | $B_{\text{mes}}/\text{nT}$ |
|---|---|---|---|
| R1 | 4.9 $\pm$ 1.8 | 1.495 $\pm$ 0.003 | 1.004 $\pm$ 0.003 |
| R2 | 2.5 $\pm$ 0.9 | 0.763 $\pm$ 0.002 | 0.517 $\pm$ 0.003 |
| R3 | 0.8 $\pm$ 0.3 | 0.2573 $\pm$ 0.0007 | 0.218 $\pm$ 0.002 |
| R4 | 0.49 $\pm$ 0.18 | 0.1507 $\pm$ 0.0004 | 0.1193 $\pm$ 0.0019 |
| R5 | 0.25 $\pm$ 0.09 | 0.0769 $\pm$ 0.0002 | 0.0958 $\pm$ 0.0018 |

Table 6: Comparison of the obtained magnetic field strengths.

| Resistor | $p_{\text{theo}}/\text{nA}\,\text{m}^2$ | $p_{\text{mes}}/\text{nA}\,\text{m}^2$ | $p_{2,\text{mes}}/\text{nA}\,\text{m}^2$ |
|---|---|---|---|
| R1 | 660 $\pm$ 40 | 140 $\pm$ 30 | 430 $\pm$ 70 |
| R2 | 336 $\pm$ 18 | 70 $\pm$ 16 | 220 $\pm$ 30 |
| R3 | 113 $\pm$ 6 | 29 $\pm$ 7 | 90 $\pm$ 15 |
| R4 | 66 $\pm$ 4 | 16 $\pm$ 3 | 50 $\pm$ 8 |
| R5 | 33.9 $\pm$ 1.9 | 13 $\pm$ 3 | 40 $\pm$ 6 |

Table 7: Comparison of the obtained magnetic dipole moments.

The theoretical values calculated with the smaller $z$ for the magnetic field strength and the measured values deviate from each other by 2 to 3 standard deviations. However, this is due to the large error of the theoretical values, which all have a relative error of over 30 %. The theoretical values calculated with $z_2$ and measured values deviate from 10 to over 100 standard deviations. But the relative errors on these values are also very small and are all below 0.3 %.

For the magnetic dipole moments, the theoretical values and the measured values calculated with the smaller $z$ differ between 6 and 14 standard deviations. The measured values, calculated with $z_2$, deviate from the theoretical values with 2 to 3 standard deviations. Altogether, it can be said that the number of standard

deviations with which the theoretical and measured values diverge does not plausibly verify one or the other distance $z$ due to the strong varying relative errors. However, if we look at the absolute values we see that the values fit together much better when using $z_2$. This could either be a coincidence and that a wrongly determined distance compensates other errors. On the other hand it could also indicate that the position marked on the cylinder does not correspond to the actual position of the conductor loop in the cylinder. In any case, it shows how strongly the distance influences the results, what is to be expected since it is cubically included in the equations (cf. eq. (12)). Thus, the determination of the distance can probably also be regarded as the largest error influence for the measurement. This is reinforced by the fact that the distance cannot be measured directly, but other lengths have to be measured outside of the cylinder and from these the distance between conductor loop and SQUID sensor can be calculated.

Other sources of error can be due to an external magnetic field, which interferes with the signal or also the fact that the samples were not pushed directly below the SQUID sensor, but rather a little too far or too short. This would also cause the measured and calculated magnetic field to diverge. For the conductor loop, it should be noted that we assumed it to be perfectly circular for the theoretical calculation. However, it appears almost oval shaped, which makes it difficult determine its area and also changes the magnetic field generated by the conductor loop. Finally, it is surprising that the theoretical and measured values for higher resistances do not differ significantly more as for low resistances although the signals are much worse for the high resistances, as described above.

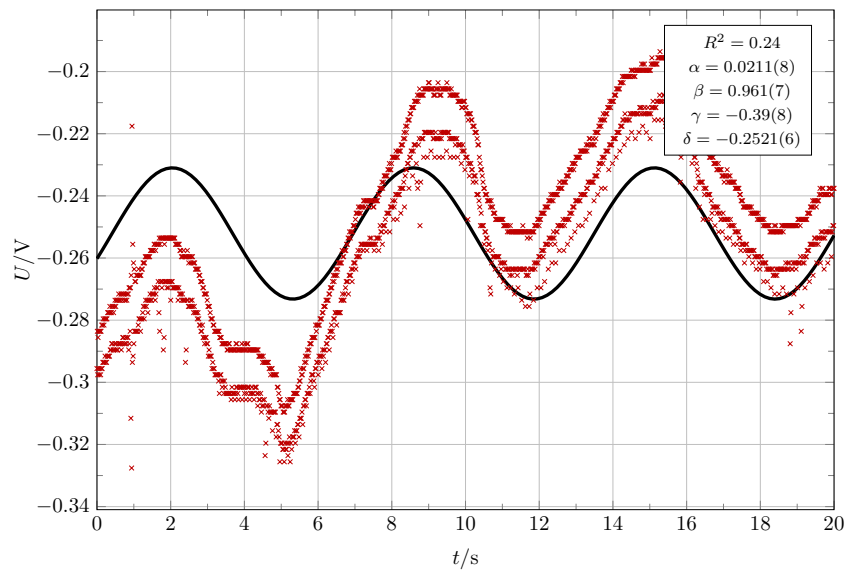# A   Appendix

# List of Figures

# List of Tables

(a) The measured data and the applied sinus fit.



(b) The polar plot of the angle $\alpha$ over the respective magnetic field strength.

Figure 5: The plots for the measurement with R1 and $\omega = 5$.
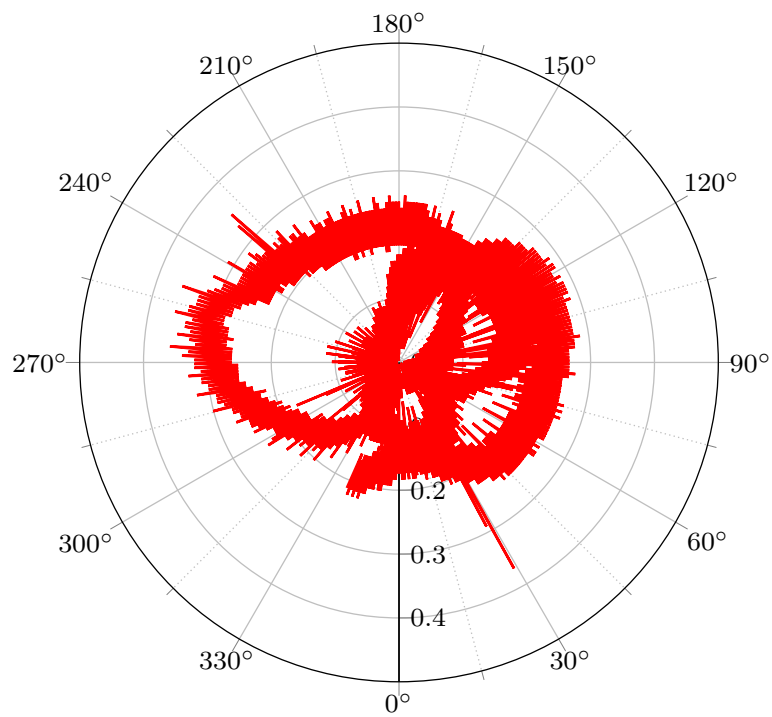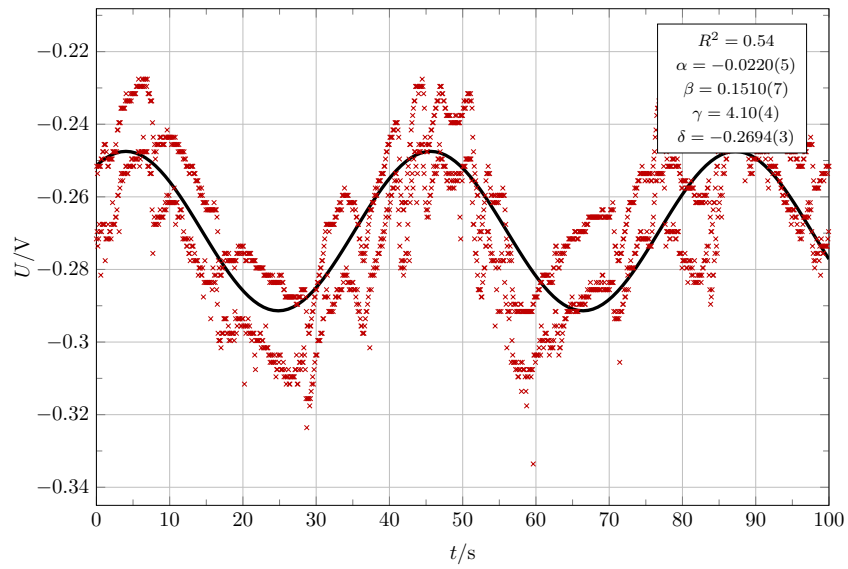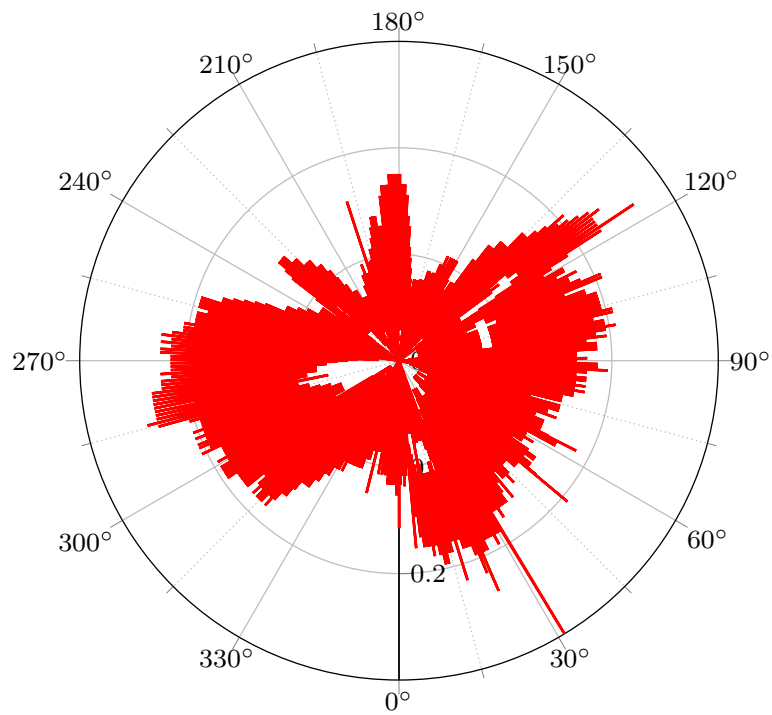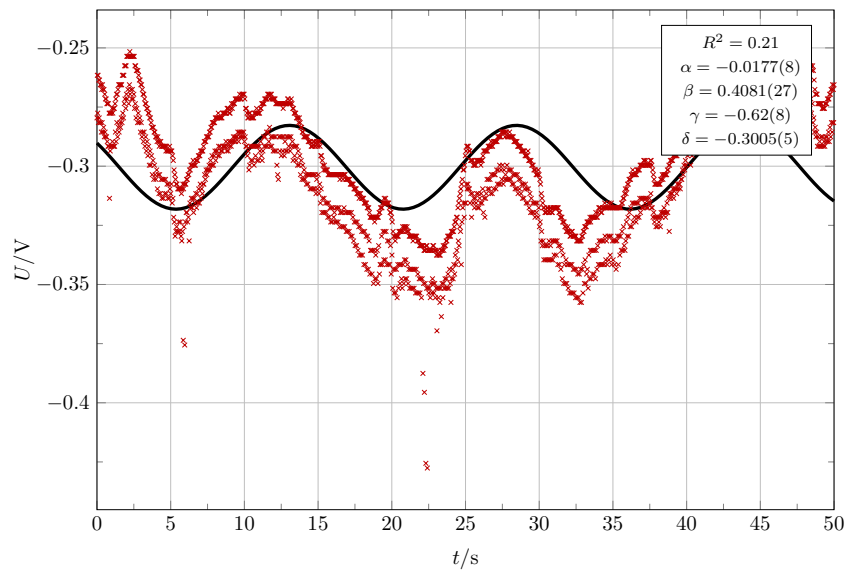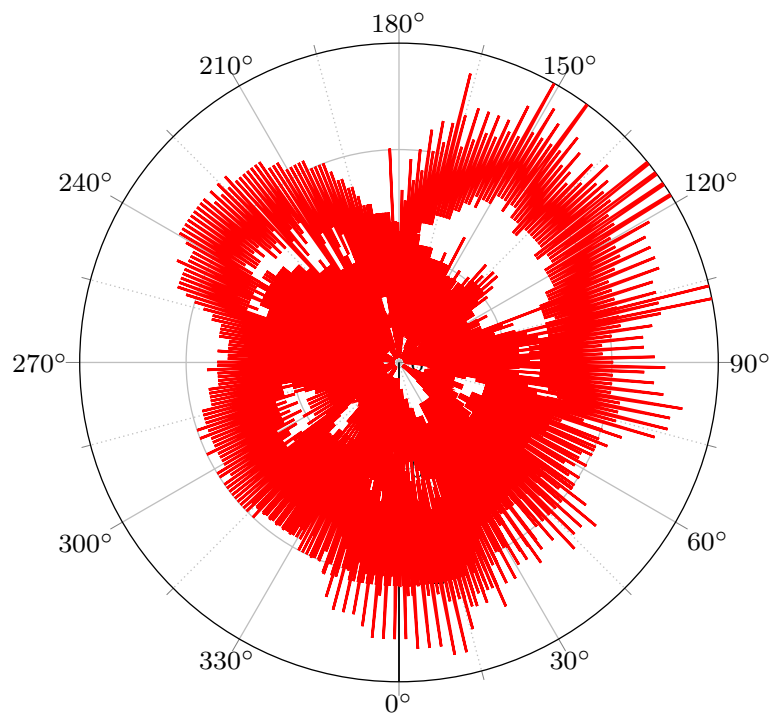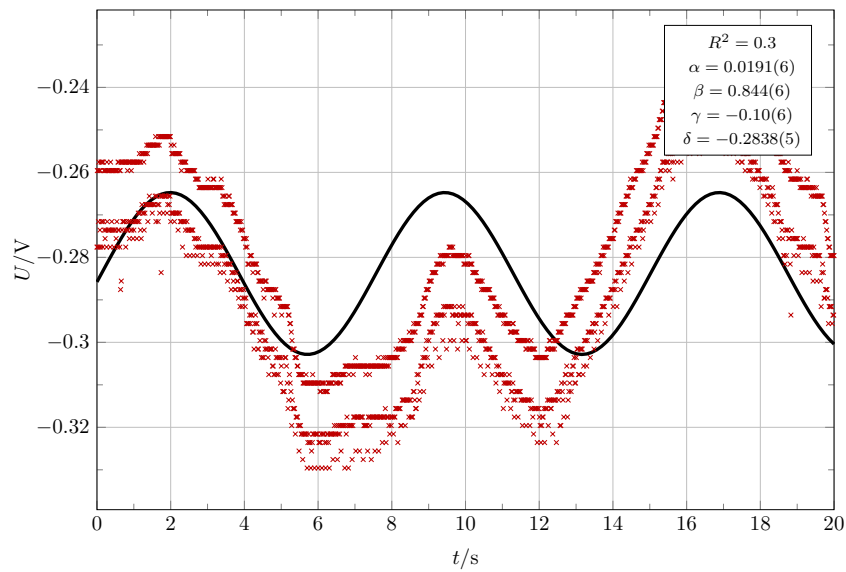
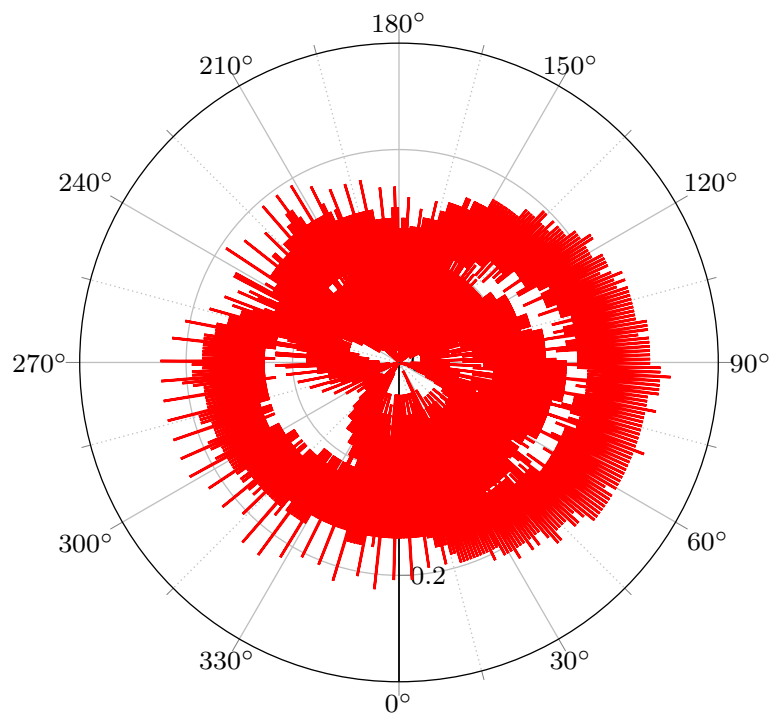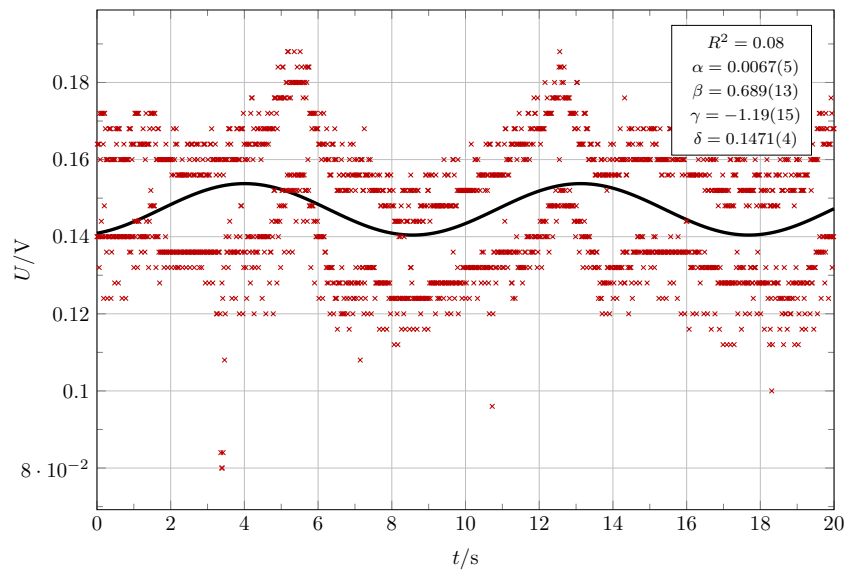(a) The measured data and the applied sinus fit.



(b) The polar plot of the angle $\alpha$ over the respective magnetic field strength.

Figure 6: The plots for the measurement with R1 and $\omega = 10$.
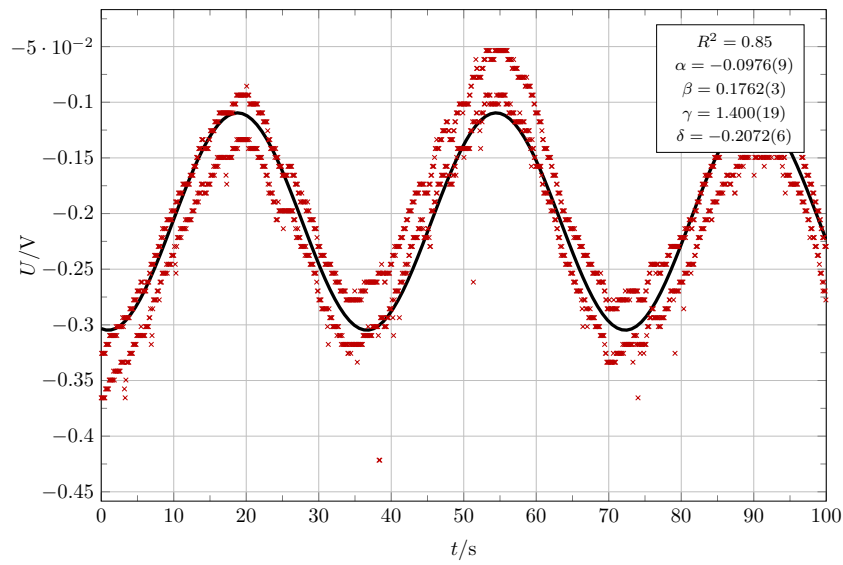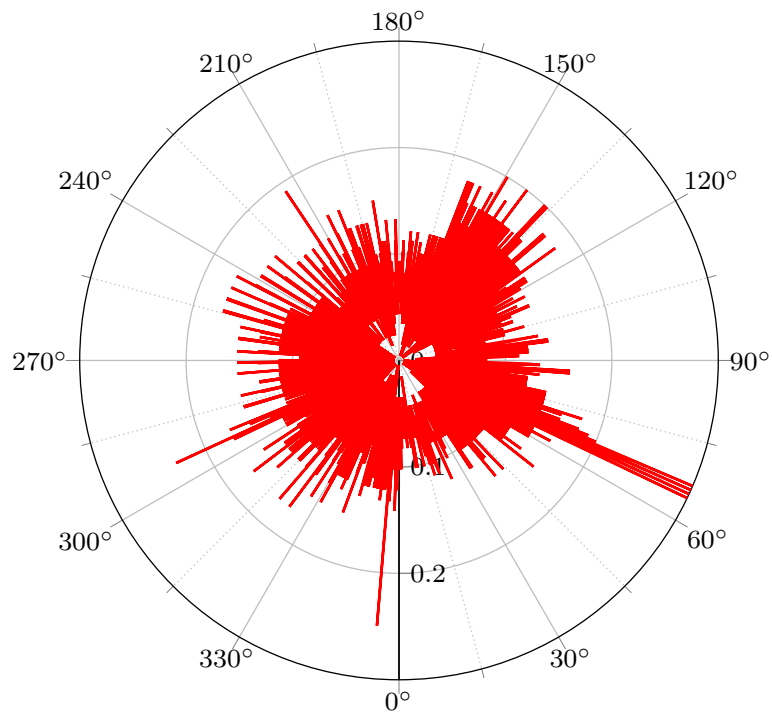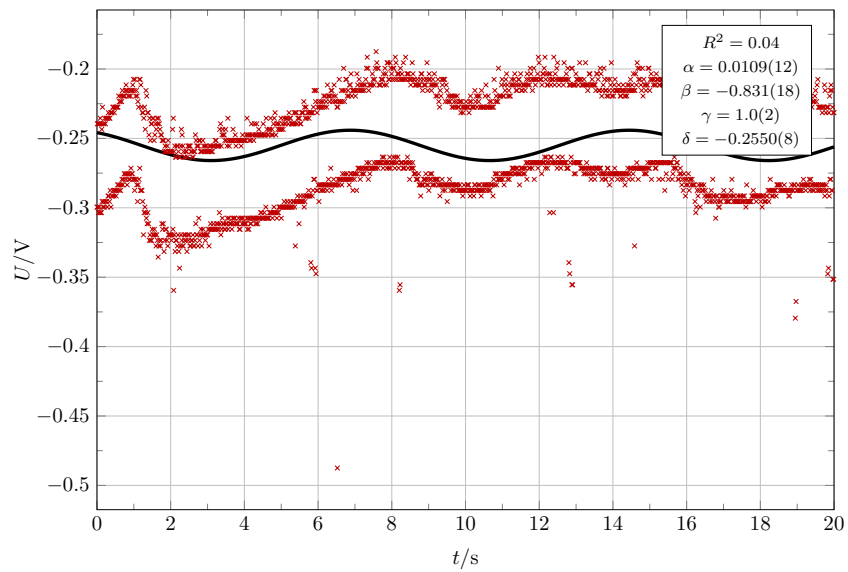
(a) The measured data and the applied sinus fit.
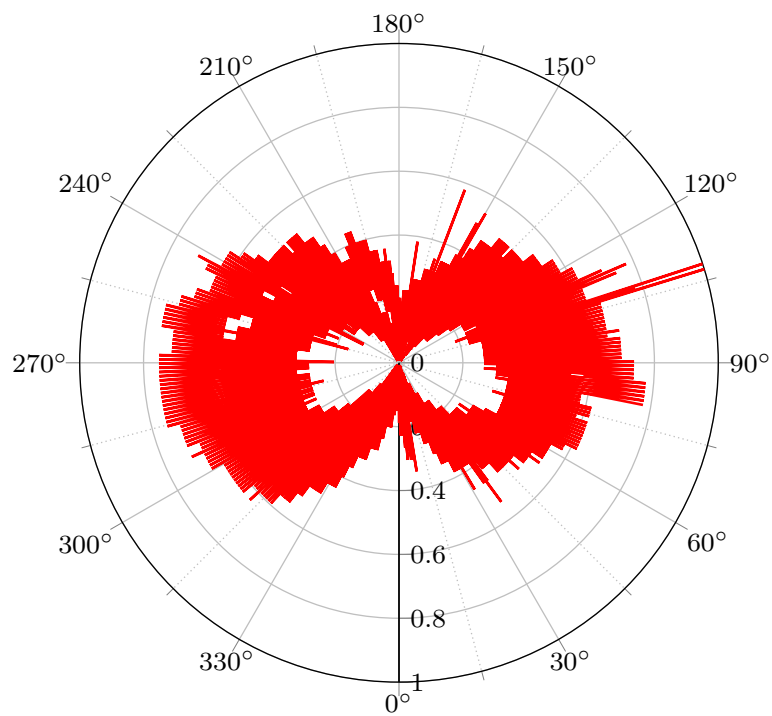


(b) The polar plot of the angle $\alpha$ over the respective magnetic field strength.

Figure 7: The plots for the measurement with R2 and $\omega = 2$.
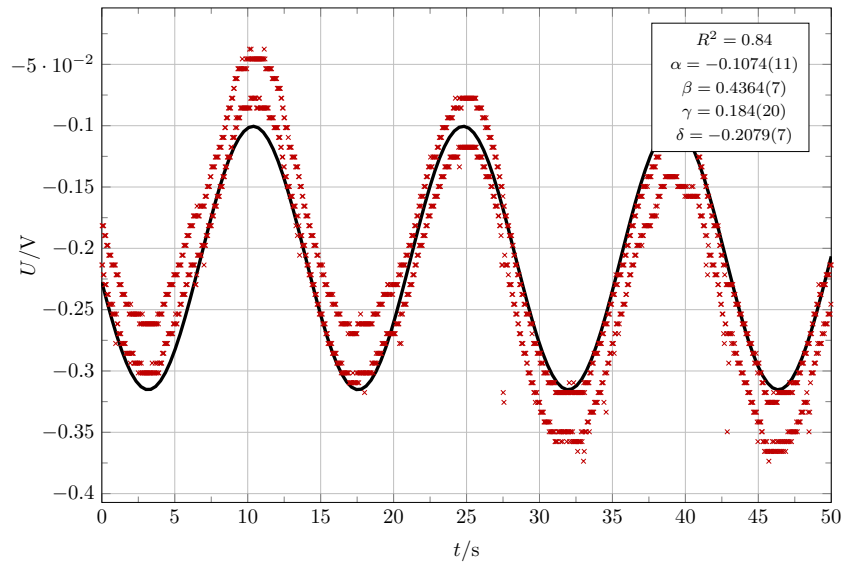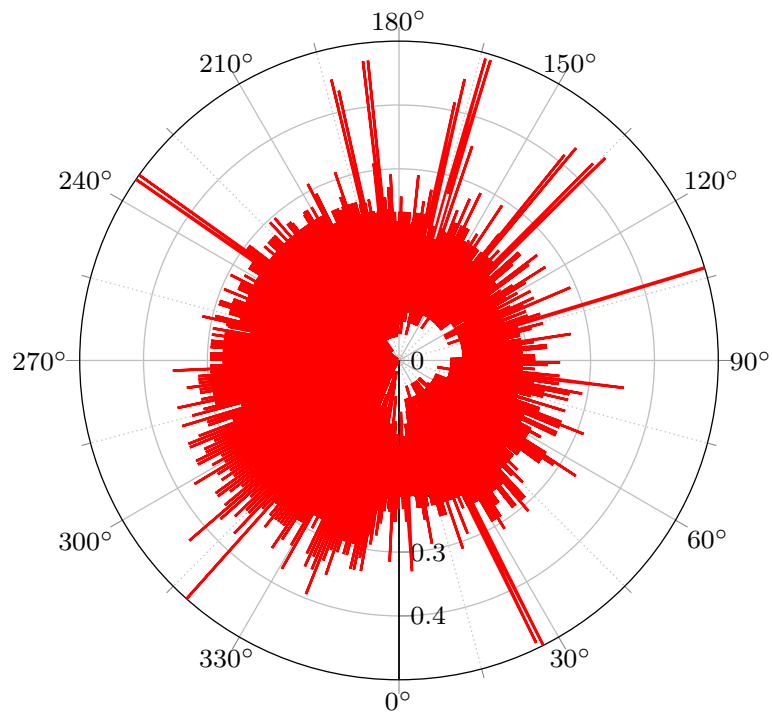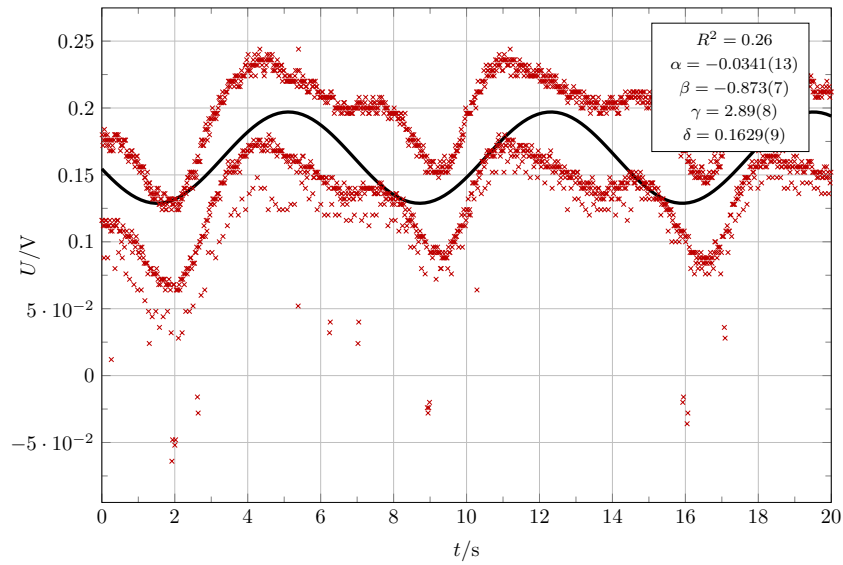
(a) The measured data and the applied sinus fit.
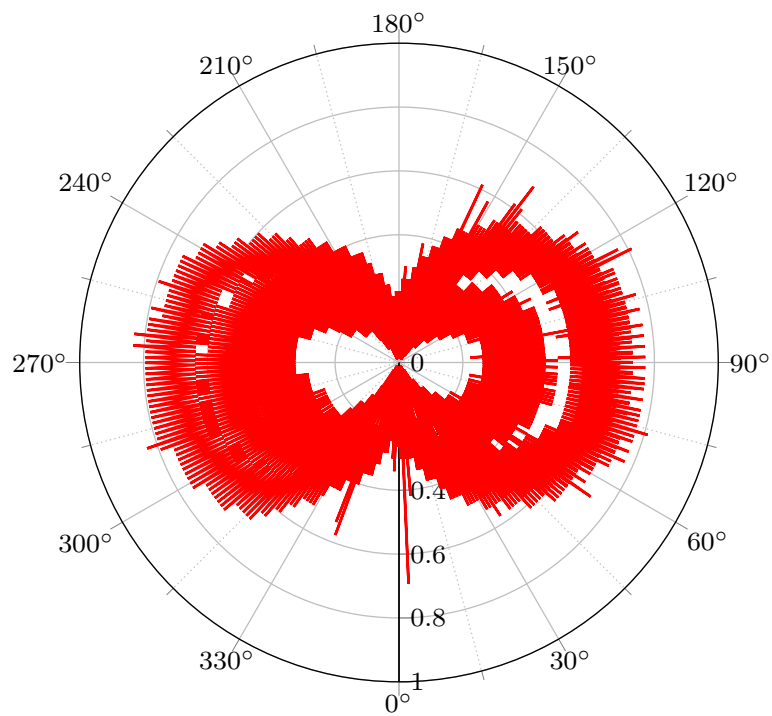


(b) The polar plot of the angle $\alpha$ over the respective magnetic field strength.

Figure 8: The plots for the measurement with R2 and $\omega = 5$.
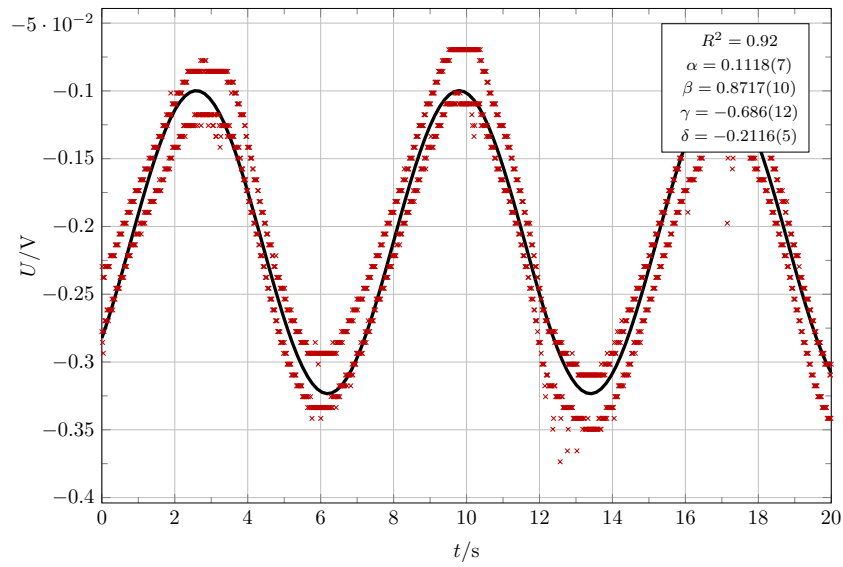
(a) The measured data and the applied sinus fit.
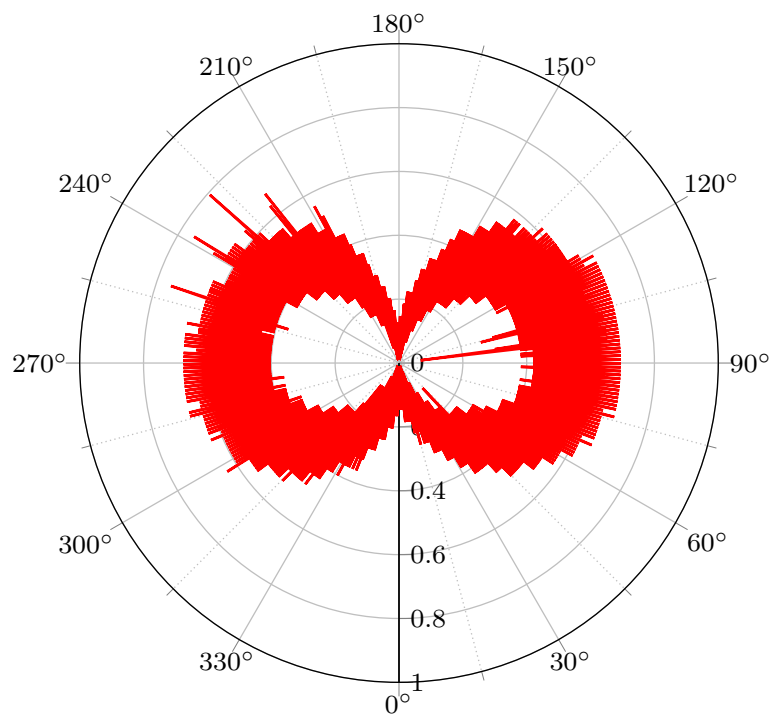


(b) The polar plot of the angle $\alpha$ over the respective magnetic field strength.

Figure 9: The plots for the measurement with R2 and $\omega = 10$.
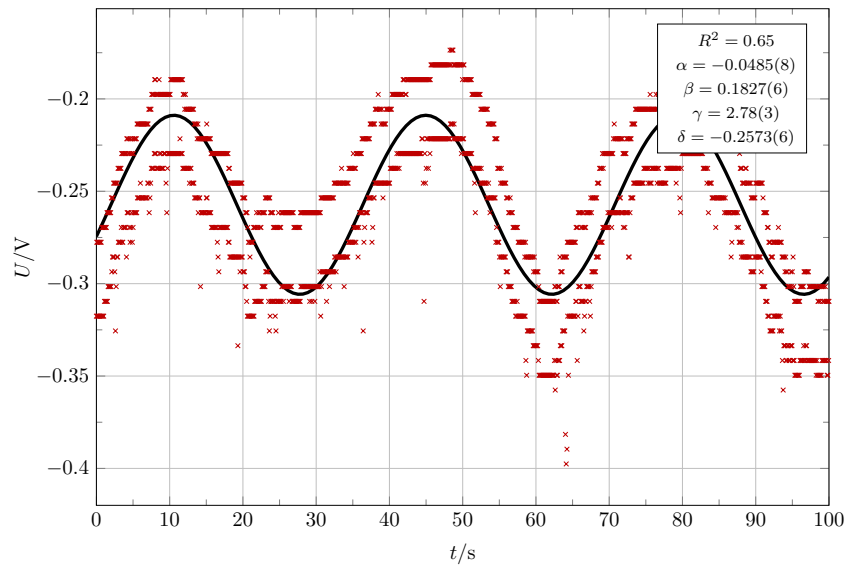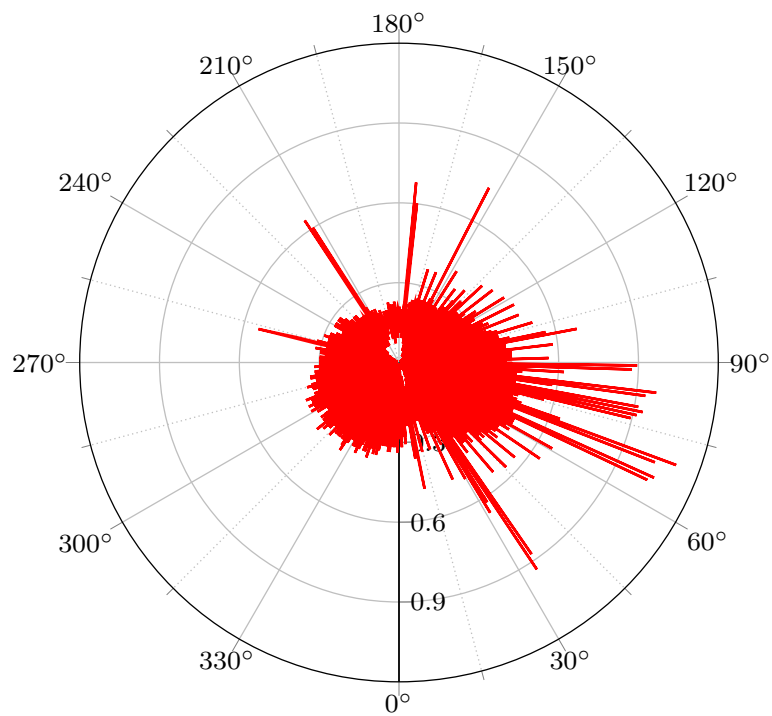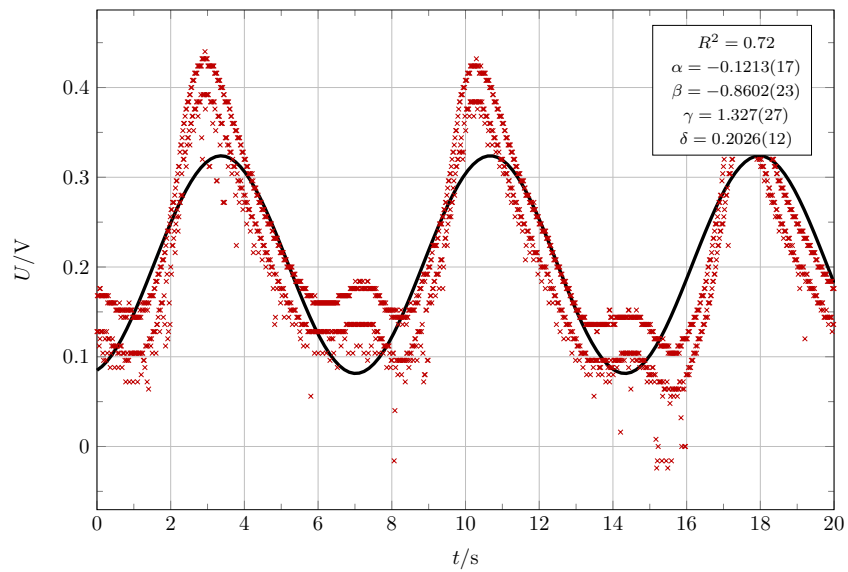
(a) The measured data and the applied sinus fit.
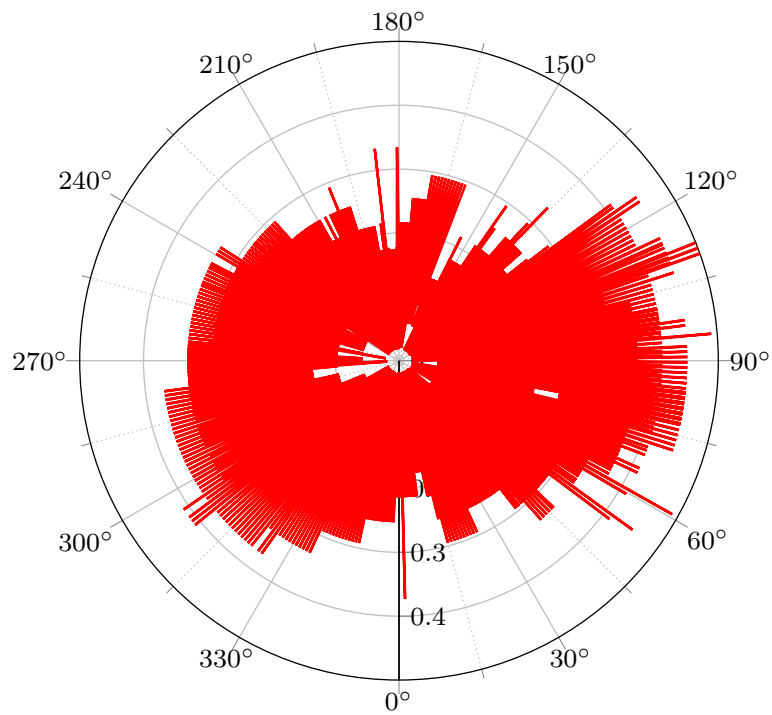


(b) The polar plot of the angle $\alpha$ over the respective magnetic field strength.

Figure 10: The plots for the measurement with R3 and $\omega = 2$.
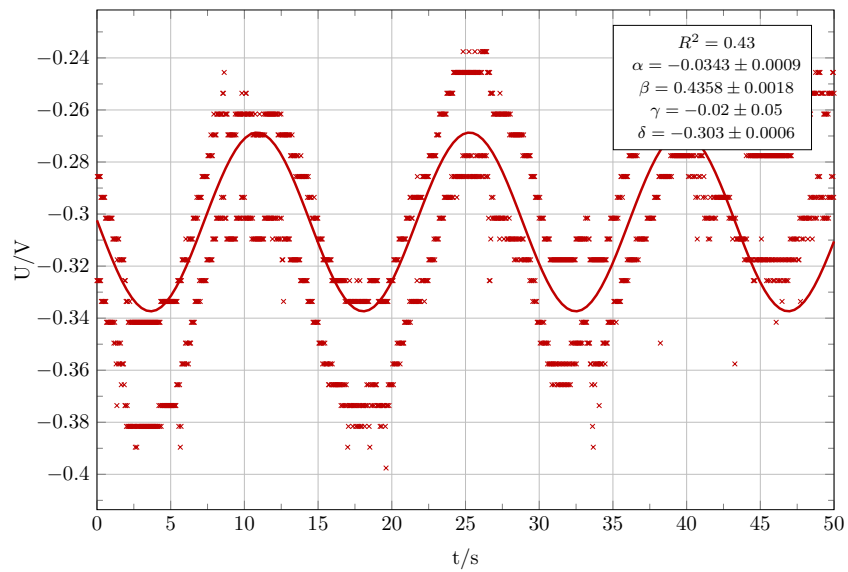
(a) The measured data and the applied sinus fit.
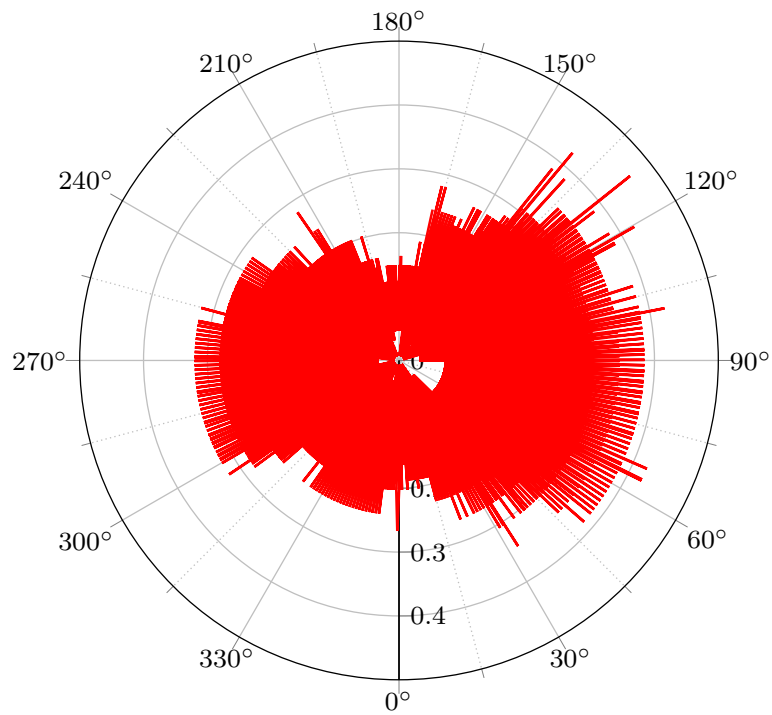


(b) The polar plot of the angle $\alpha$ over the respective magnetic field strength.

Figure 11: The plots for the measurement with R3 and $\omega = 5$.
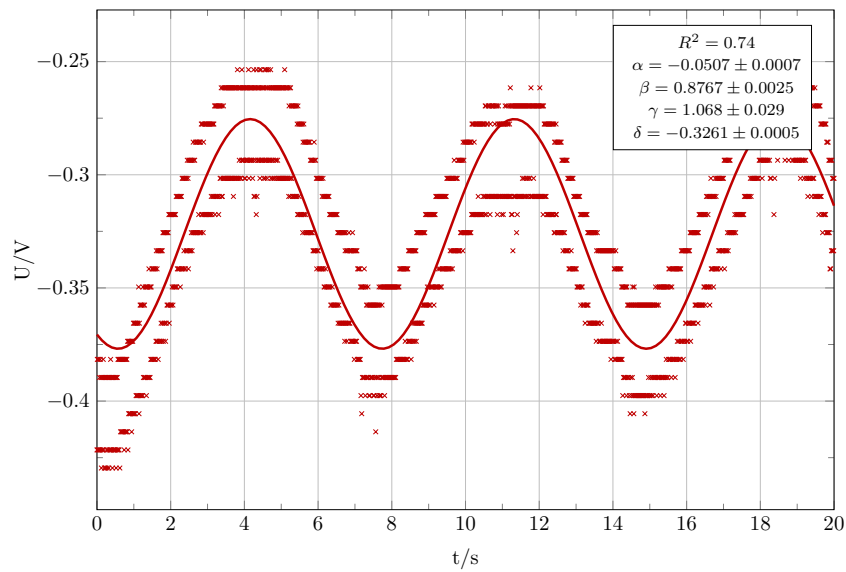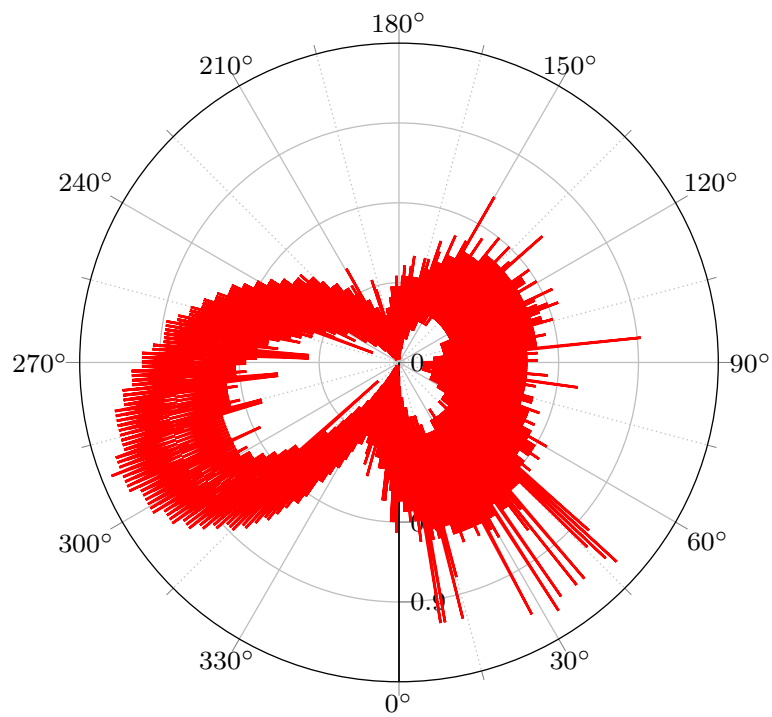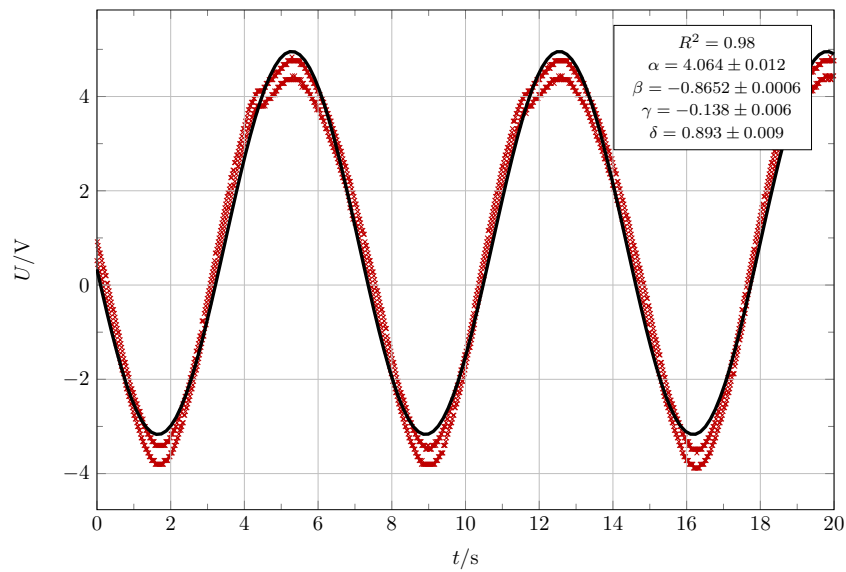
(a) The measured data and the applied sinus fit.
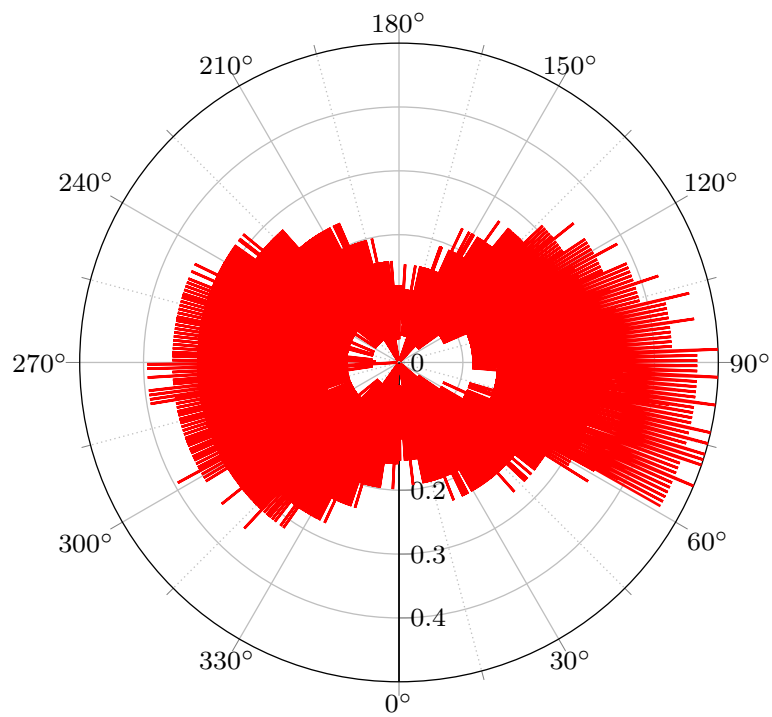


(b) The polar plot of the angle $\alpha$ over the respective magnetic field strength.

Figure 12: The plots for the measurement with R3 and $\omega = 5$.
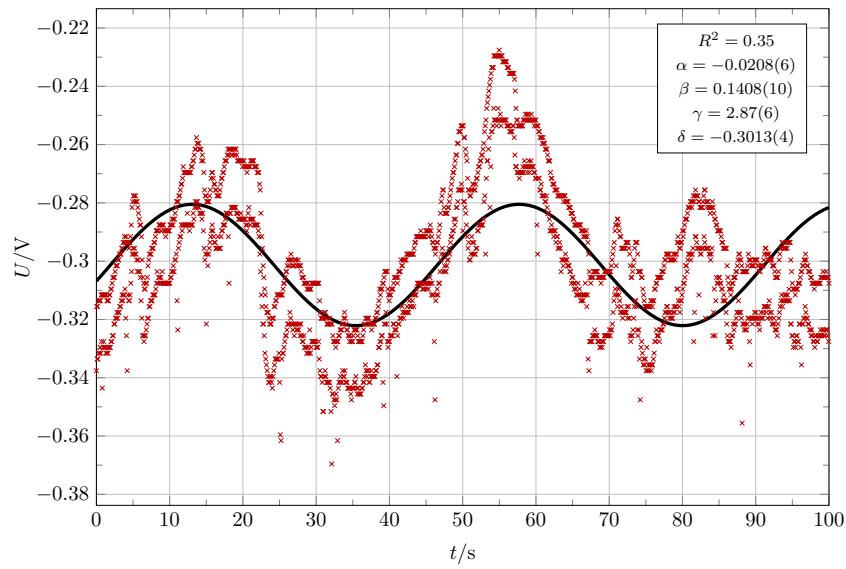
(a) The measured data and the applied sinus fit.
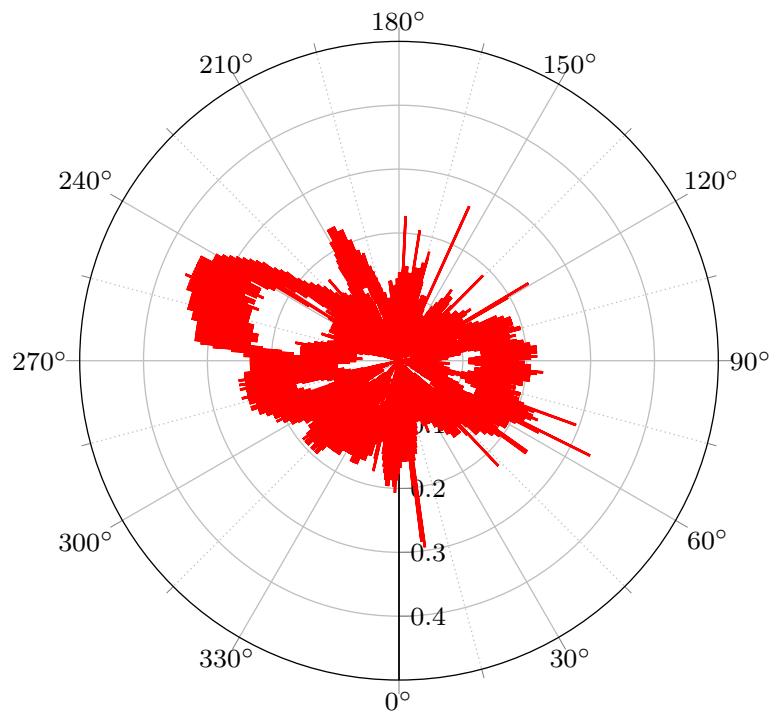


(b) The polar plot of the angle $\alpha$ over the respective magnetic field strength.

Figure 13: The plots for the measurement with R4 and $\omega = 2$.
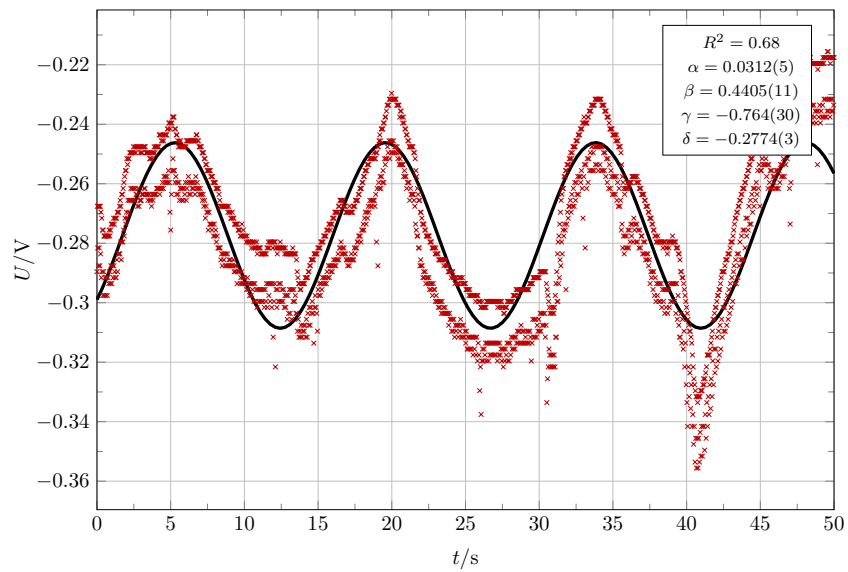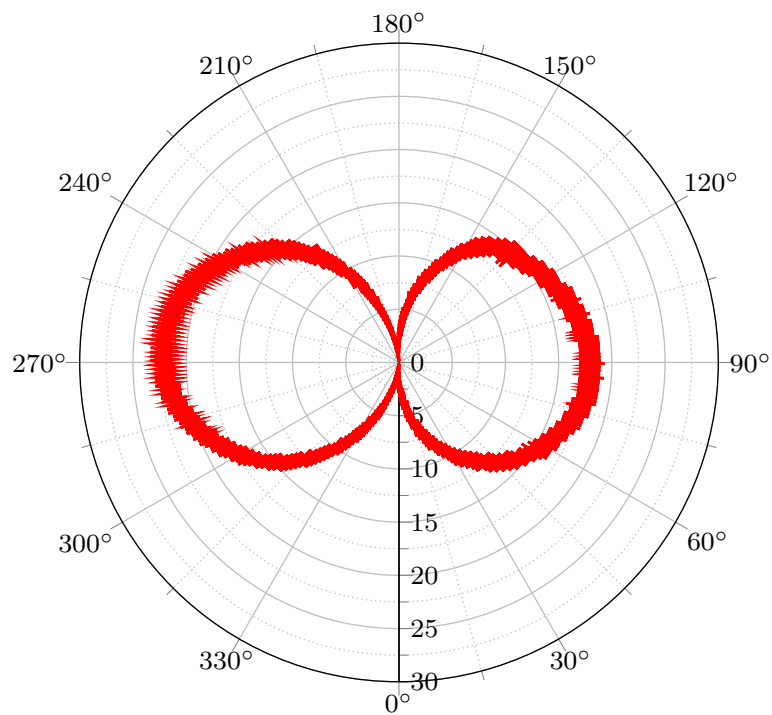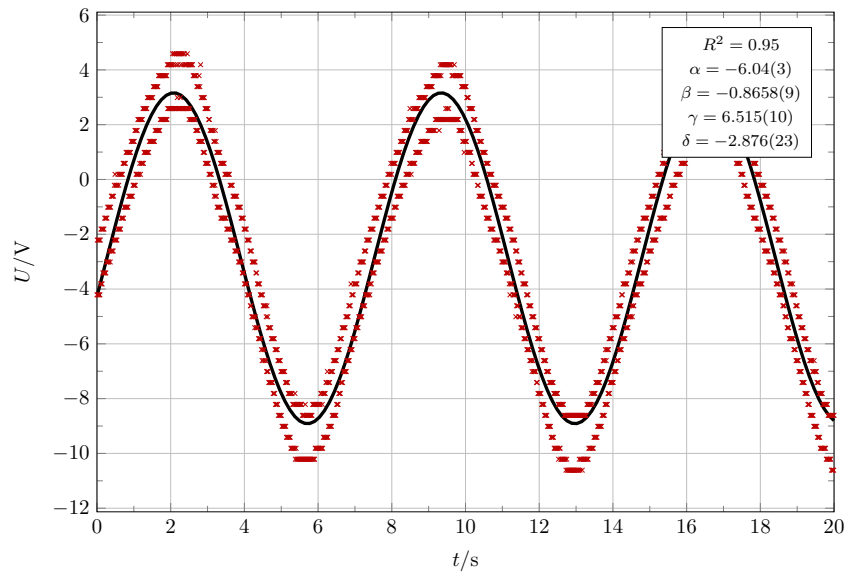
(a) The measured data and the applied sinus fit.
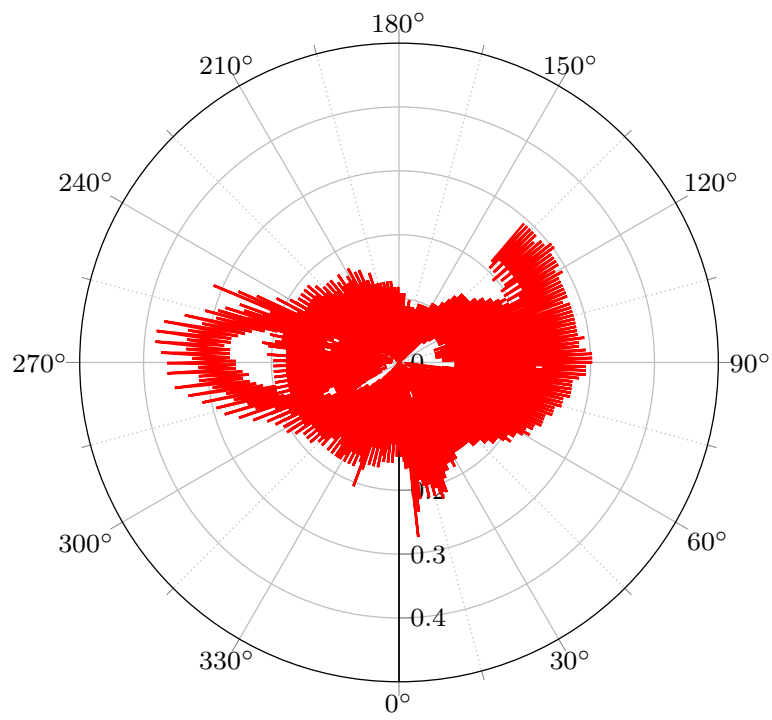


(b) The polar plot of the angle $\alpha$ over the respective magnetic field strength.

Figure 14: The plots for the measurement with R4 and $\omega = 5$.

(a) The measured data and the applied sinus fit.



(b) The polar plot of the angle $\alpha$ over the respective magnetic field strength.

Figure 15: The plots for the measurement with R4 and $\omega = 10$.
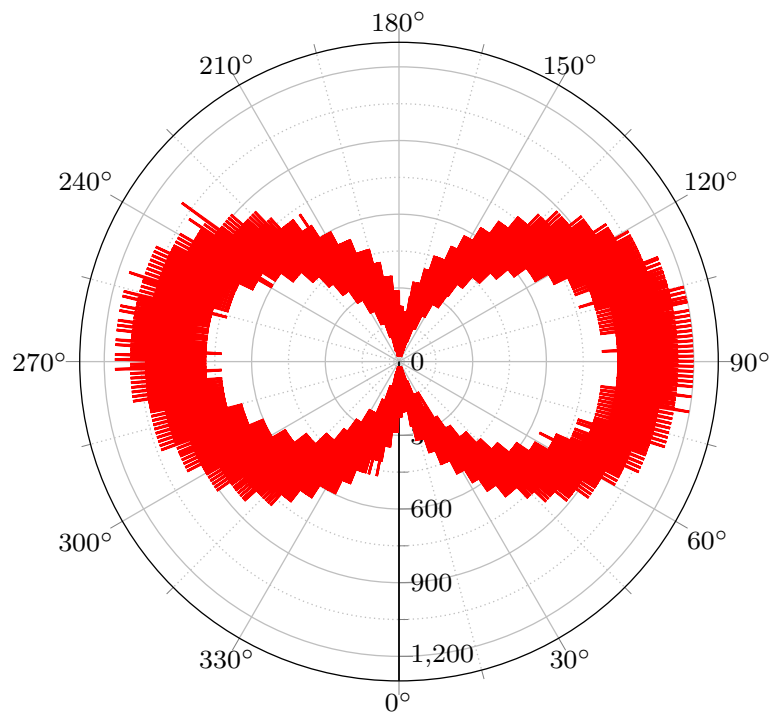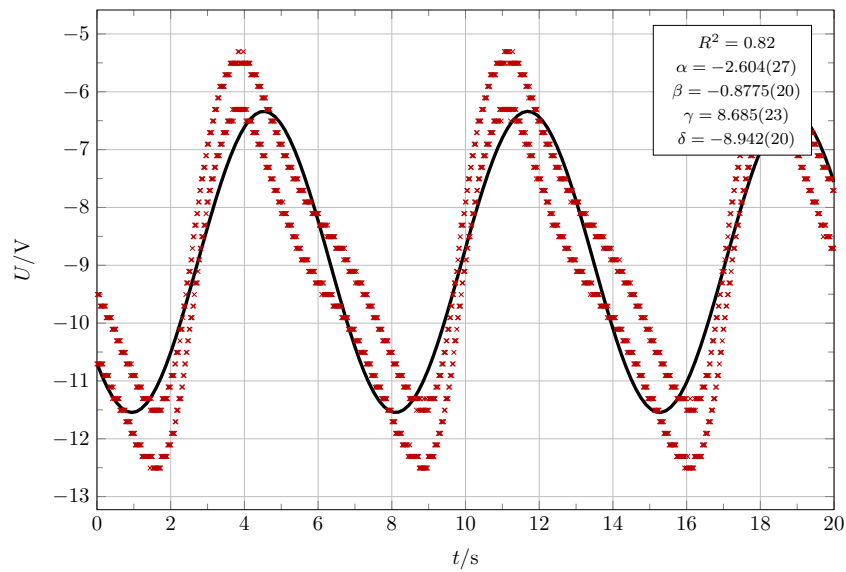
(a) The measured data and the applied sinus fit.



(b) The polar plot of the angle $\alpha$ over the respective magnetic field strength.

Figure 16: The plots for the measurement with R5 and $\omega = 2$.

(a) The measured data and the applied sinus fit.



(b) The polar plot of the angle $\alpha$ over the respective magnetic field strength.

Figure 17: The plots for the measurement with R5 and $\omega = 5$.
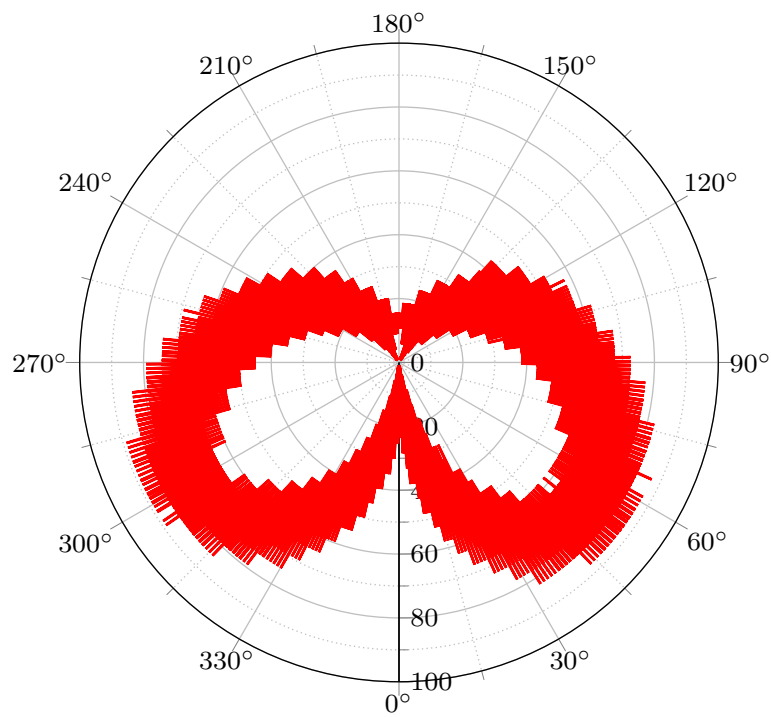
(a) The measured data and the applied sinus fit.



(b) The polar plot of the angle $\alpha$ over the respective magnetic field strength.

Figure 18: The plots for the measurement with R5 and $\omega = 10$.

(a) The measured data and the applied sinus fit.



(b) The polar plot of the angle $\alpha$ over the respective magnetic field strength.

Figure 19: The plots for the measurement of the iron span.

(a) The measured data and the applied sinus fit.



(b) The polar plot of the angle $\alpha$ over the respective magnetic field strength.

Figure 20: The plots for the measurement of the gold sample.

(a) The measured data and the applied sinus fit.



(b) The polar plot of the angle $\alpha$ over the respective magnetic field strength.

Figure 21: The plots for the measurement of the gray stone.

(a) The measured data and the applied sinus fit.



(b) The polar plot of the angle $\alpha$ over the respective magnetic field strength.

Figure 22: The plots for the measurement of the red stone.

(a) The measured data and the applied sinus fit.



(b) The polar plot of the angle $\alpha$ over the respective magnetic field strength.

Figure 23: The plots for the measurement of the magnetic span.

(a) The measured data and the applied sinus fit.



(b) The polar plot of the angle $\alpha$ over the respective magnetic field strength.

Figure 24: The plots for the measurement of the crown cap.

(a) The measured data and the applied sinus fit.



(b) The polar plot of the angle $\alpha$ over the respective magnetic field strength.

Figure 25: The plots for the measurement of the iron stick.

## A.1 Laborheft

# Bibliography

[1] BANGE, Volker: *Einrichtung des Versuches „SQUID".* 2000

[2] KÖHLI, M.: *Versuchsanleitung Fortgeschrittenen Praktikum Teil I – Superconducting Quantum Interference Device.* 2011